Materials Research Express

PAPER

Low pressure chemical vapor deposition synthesis of large area hetero-doped mono- and few- layer graphene with nitrogen and oxygen species

To cite this article: Maria Hasan *et al* 2019 *Mater. Res. Express* **6** 055604

Materials Research Express

PAPER

Low pressure chemical vapor deposition synthesis of large area hetero-doped mono- and few- layer graphene with nitrogen and oxygen species

RECEIVED
9 November 2018

REVISED
27 January 2019

ACCEPTED FOR PUBLICATION
12 February 2019

PUBLISHED
22 February 2019

Maria Hasan[1,7], **Wang Meiou**[2], **Liu Yulian**[2], **Huy Q Ta**[2], **Liang Zhao**[2,3], **Rafael G Mendes**[4], **Stefan Oswald**[4], **Zareen Akhter**[6], **Zahida P Malik**[7], **Nasir M Ahmad**[8], **Zhongfan Liu**[1] and **Mark H Rümmeli**[2,3,4,5]

[1] College of Chemistry & Molecular Engineering, Peking University, Beijing 100871, People's Republic of China
[2] College of Energy, Soochow Institute for Energy and Materials Innovations, Soochow University, Suzhou 215006, People's Republic of China
[3] Key Laboratory of Advanced Carbon Materials and Wearable Energy Technologies of Jiangsu Province, Soochow University, Suzhou, 215006, People's Republic of China
[4] IFW Dresden, 20 Helmholtz Strasse, Dresden 01069, Germany
[5] Centre of Polymer and Carbon Materials, Polish Academy of Sciences, M Curie-Sklodowskiej 34, Zabrze 41-819, Poland
[6] Department of Chemistry, Quaid-I-Azam University, Islamabad 45320, Pakistan
[7] School of Natural Sciences, National University of Sciences and Technology, Islamabad 44000, Pakistan
[8] School of Chemical and Material Engineering, National University of Sciences and Technology, Islamabad 44000, Pakistan

E-mail: mhr1967@yahoo.com

Keywords: hetero-doped graphene, powder precursor, CVD, rapid growth

Supplementary material for this article is available online

Abstract

The doping graphene helps breaks its surface inertness providing it an intrinsic degree of catalytic activity. While single elemental doping of graphene (e.g. with N) enhances its catalytic potential, the current trend is to develop graphene doped with multiple elements. These heterodoped graphene species have improved electro-catalytic activities as compared to their corresponding single heteroatom doped counterparts because of strong charge redistribution and synergistic effects due to differences in the dopant electro-negativities. Hence, they are better suited for multiple catalytic reactions to better cope with reaction intermediates. Never-the-less, to date only a few examples exist. In this work we show it is possible to synthesize in a single CVD step, large area single- and few- layer graphene doped with oxygen and nitrogen species. Moreover, this is achieved using a solid precursor in a pure H_2 environment with growth being achieved in under 5 min.

1. Introduction

Electrocatalysts are typically based on expensive transition metals. Therefore, from economic considerations it is important to develop metal free electrocatalysts such as those based on carbon. However, carbon based catalysts better suit heterogeneous catalysis. Nevertheless, this limitation can be overcome by reducing the dimensions to the nanometer scale and/or decreasing the layer number of carbon based materials [1]. Graphene has a myriad of fascinating physical properties [2] yet pristine graphene is chemically inert and a zero band gap material that limits its applications in electrocatalysis and the semiconductor industry. Introducing vacancies and defects into the hexagonal carbon framework of graphene through heteroatom doping can not only open up graphene's band gap but also breaks its surface inertness providing it an intrinsic degree of catalytic activity [3]. In fact, the most widely studied heterodoped carbon based material in catalysis is graphene oxide. However, it often contains impurities and amorphous debris that block vacancies and defects that are the active sites for catalysis [4]. Therefore, hetero-doped graphene that possess properties such as a large active surface area, single atom thick layers, chemically stability, purity, crystallinity and electrical conductivity can provide a superior materials choice for both heterogeneous and homogenous electrocatalysis [5].

Table 1. Hetero-doped Graphene through CVD synthesis reactions in the literature and this work.

Hetero dopants	CVD	Flow gas	Precursor	Layer number	Substrate	References
P and N	APCVD	Ar	$(NH_4)_3PO_4$, CH_4	Few layer	MgO	[9]
S and N	APCVD	N_2	Pyrimidine thiophene	Few layer	Fe-Co/Al_2O_3	[10]
B and N	LPCVD	Ar, H_2	NH_3-BH_3, CH_4	Few layer	Cu	[11]
BN domains	LPCVD	H_2, N_2	CH_4, Boric acid, N_2	Monolayer (or few)	Cu	[12]
O and N	LPCVD	H_2	Nitrophenyl Ferrocene	Monolayer	Cu	This work

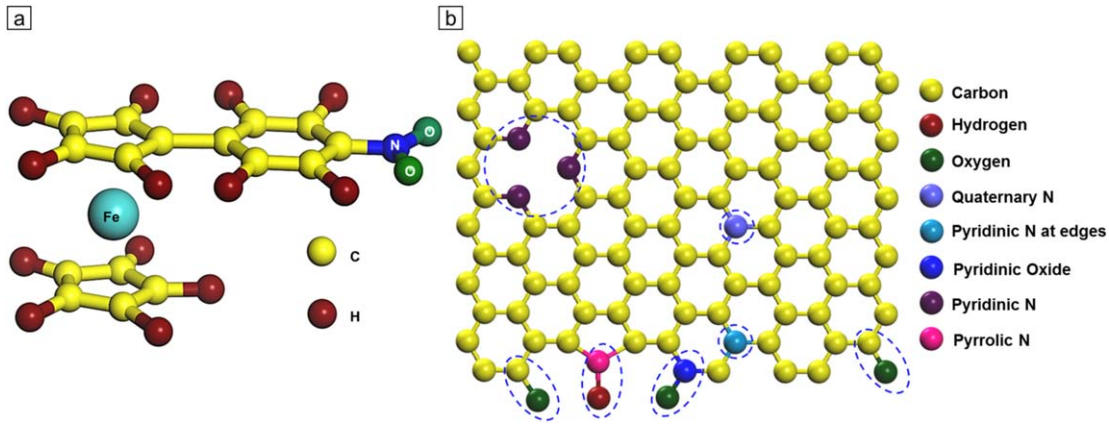

Figure 1. (a) Ball and stick model for nitrophenyl ferrocene precursor molecule. (b) Stick and ball model showing various configurations for the hetero-doped graphene configurations obtained in this work .

N doping has the ability to donate electrons to adjacent carbon atoms that results in an 'activation region' on graphene surface and can directly participate in catalysis. Being a close neighbor of carbon, nitrogen doping in graphene improves its electro catalytic performance without considerably disturbing its two dimensional planar symmetry required for large surface area property [6]. In addition, the presence of oxygen in graphene (in form of graphene oxide) can also make graphene catalytically active [7]. The new emerging trend in electrocatalysis is to dope graphene with two or more heteroatoms. These heterodoped graphene species have improved electro-catalytic activities as compared to their corresponding single heteroatom doped counterparts because of strong charge redistribution and synergistic effects due to differences in the dopant electronegativities [8]. Nevertheless, the idea of multi-elemental doping has to date hardly been explored in graphene (See table 1) [9–12]. There are only a handful of examples where hetero-doped combinations like boron and nitrogen [13] nitrogen and phosphorous [14] nitrogen and sulphur [15] have been developed and which exhibit comparatively higher oxygen reduction reaction (ORR) performance as compared to other graphene derivatives, *viz.*, enhanced catalytic performance as compared to single element doping [16]. Thus, the synthesis and exploration of new hetero-doped combinations in graphene sheets is important. The combination of nitrogen and oxygen functionalities tested in mesoporous carbon and hydrogels have shown high electro-catalytic activity towards ORR and oxygen evolution reaction (OER) respectively [17, 18]. However, such a combination of oxygen and nitrogen based species in hetero-doped graphene sheets has yet to be demonstrated.

Herein, we report synthesis of monolayer graphene hetero-doped with oxygen and nitrogen species in the form of carbonyls, hydroxyls, NO, pyridinic N and graphitic N, *viz*, N and O hetero-doped graphene, for the first time. This is achieved using a *single solid precursor* of nitrophenyl ferrocene in the presence of H_2 (See figure 1).

The synthesis of our multi-doped graphene takes place in a single step low pressure chemical vapor deposition (LPCVD) reaction. Unlike the previous CVD synthesis approaches for hetero-doped graphene, our precursor simultaneously provides a source of O, N and C for large area hetero-doped mono-layer and few-layer graphene synthesis. (Figure S1 is available online at stacks.iop.org/MRX/6/055604/mmedia) Contrary to conventional methods such as ball milling and hydrothermal used for synthesizing hetero-doped graphene [19, 20] CVD synthesis can provide a scalable and crystalline product. Moreover, we have investigated the effects of (i) the CVD reactor tube configuration (figure 2) (ii) optimized precursor amounts (iii) reaction time (iv) and temperature optimization to better elucidated the growth mechanisms involved and provide layer number and doping control.

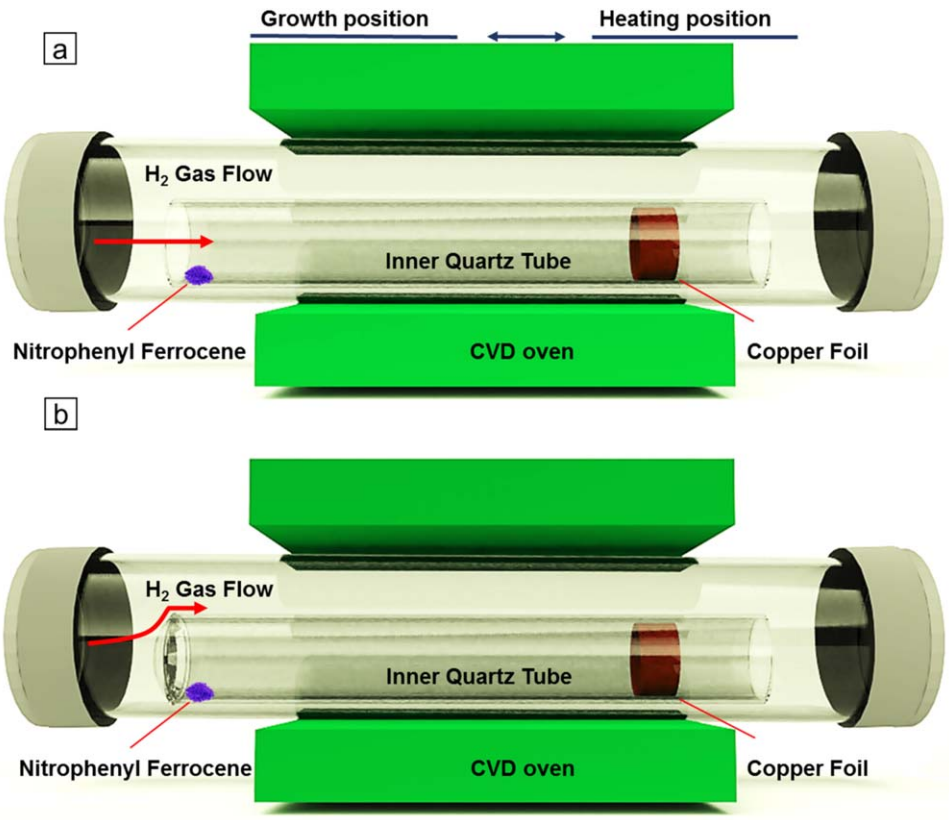

Figure 2. Schematic illustrating the sliding oven LPCVD set up positioned during growth (dimensions are not to scale). (a) fully open inner quartz tube. (b) Half closed inner quartz tube.

We demonstrate these aspects through Raman spectroscopy, scanning electron microscopy, high resolution transmission electron microscopy (HRTEM), x-ray photoelectron spectroscopy (XPS), electron energy loss spectroscopy (EELS) and Fourier-transform infrared spectroscopic (FTIR) characterizations.

2. Experimental methods

2.1. Graphene growth

The CVD synthesis of Heterodoped graphene was carried out in a horizontal tube furnace at low pressure (0.5 mbar). A 25 μm thick copper foil (45 mm $\times$ 10 mm) was used as a substrate to grow hetero-doped graphene films. The ability of Ferrocene as a sole source for both carbon feed stock and catalytic Fe particles has been explored for carbon nanotubes and graphene production [21, 22]. There are numerous ways to derive ferrocene in few steps and thus to tailor its elemental constituency according to nature of product required. Here Ferrocene derivative p4-nitro phenyl Ferrocene that contained all three elements viz., N, O and C has been used for first time for heterodoped graphene synthesis. The precursor was prepared through the arylation reaction of ferrocene with diazonium salt of 4-nitroaniline in a single step synthesis [23]. When exploring use of an inner quartz reactor tube with both ends open figure 2(a) precursor amounts of 0.5 mg, 1 mg, 5 mg and 10 mg were tested, while for a half closed inner reaction tube figure 2(b) precursor amounts of 0.5 mg were sufficient (although 1 mg, 5 mg and 10 mg amounts were also explored). The precursor was placed upstream (by the closed end in the case of the half closed inner reactor tube). Close to the opening of the inner reactor tubes at the downstream end a copper strip was rolled and carefully placed inside the tube at a distance of 25 mm from its open end. The inner quartz tube was then placed inside the main CVD furnace quartz tube (50 mm diameter, 1580 mm length) (figure 2(b)). Initially the furnace was evacuated to 0.09 mbar using a vacuum rotary pump. Afterwards, the system was flushed with pure Ar (99.99%) gas at 200 standard cubic centimeters per minute (SCCM) flow. As a result, the inner pressure raised to 0.9 mbar. This flushing was performed for 30 min (60 and 120 min durations showed no gain as opposed to 30 min). After 30 min the flow of Ar was stopped and a pure H_2 (99.99%) flow at 16 SCCM was started (at a pressure of 0.5 mbar). The furnace was heated to 1025 °C at the rate of 23 °C min^{-1}. During these steps the oven stayed at position away from the precursor as shown in figure 2. Once the reaction temperature was reached (in 45 min) the CVD oven was moved upstream to the growth

position as indicated in figure 2 so as to enable a controlled lower precursor temperature (300, 380 and 500 °C were explored, optimal growth was at 380 °C) and maintain a higher and constant reaction temperature (1025 °C). The optimum growth time, for monolayer graphene was 3 min (subsequently 5, 7, 10 min were also tested) for the half closed inner tube (no graphene was observed with an open inner tube). After growth the CVD oven was slid away from the growth region to provide rapid cooling [24]. The hydrogen flow was stopped and switched to a 200 SCCM of Ar gas flow until the furnace had cooled to room temperature. A graphical representation of the CVD reaction is shown in the supporting information in figure S1(a).

2.2. Transfer

For TEM and HRTEM studies the hetero-doped graphene was transferred on to standard lacey carbon Cu TEM grids. The protocol steps are to first spin coat PMMA solution in ethyl acetate, followed by etching the copper substrate in 0.5 molar aqueous solution of ammonium persulphate (Sigma Aldrich, purity $\geqslant$98%) for ~100 min, and thereafter rinse thoroughly in deionized water and then fish the graphene onto a standard lacey carbon Cu TEM grid after which the PMMA is removed in hot acetone vapor [25]. Finally, the TEM grid was annealed in high vacuum (10^{-6} mbar) at 200 °C for 12 h to remove any organic residue.

For SEM and Raman characterizations, SiO_2 (300 nm)/Si wafer was used as the substrate for transfer in place of a TEM grid. The wafer was first washed with pure acetone and absolute ethanol and then dried with N_2. The graphene film was fished onto it and then annealed in an oven at 75 °C for 20 min. Afterwards, pure acetone was used to remove PMMA.

2.3. Characterization

SEM measurements were performed on a Hitachi SU-8010. EELS, TEM and HRTEM were performed on a Titan^3 80–300 with a monochromator and a Cs corrector for the primary objective lens. The electron acceleration voltage was 80 kV. XPS was performed on a Thermo Fisher Scientific (model ESCALAB 250 xi). Raman spectra and Raman mapping were collected on a Horiba (Confocal LabRAM HR 800) using 633 nm laser with approximate power kept at 2 mW. The FTIR test was done on Tensor 27 spectrometer from Bruker Optics in the ATR mode. The sheet resistance was measured through a SZT-C four-probe test bench Suzhou Jingge electronics.

3. Results and discussions

When employing an inner quartz reactor tube configuration with both ends open (figure 2(a)) no graphene formation was observed even when increasing the precursor amounts from 0.5 mg, to 1, 5 mg and 10 mg. This can be attributed to a limited amount of feedstock species, as the produced species from the thermally decomposed precursor (Nitrophenyl Ferrocene) are flushed away too rapidly which not only limits the feedstock species suitable for graphene growth, but also limits the decomposition of the precursor, further limiting decomposed feedstock (carbon units) suitable for growth. In the second configuration, the upstream end of the inner quartz reaction tube is sealed (closed) as shown in figure 2(b) which we refer to as a half closed tube. This configuration allows the decomposed precursor species to slowly diffuse out of the reactor tube and thus provides sufficient time for precursor decomposition and thus graphene formation. Indeed, so efficient is this process that only 0.5 mg of precursor material is required.

Henceforth, we focus on systematic investigations using a half closed inner tube [26] for the controlled production of mono- and few- layer graphene doped with N and O species.

The electronic properties of hetero-doped graphene are strongly dependent upon its thickness (layer number) [27]. Therefore, understanding the mechanism by which layer number can be controlled is of importance. As a part of this investigation we examined the role of precursor mass while keeping all other reaction parameters constant (figure S1(a)), namely a reaction temperature of 1025 °C, a precursor temperature of 380 °C and growth duration of 3 min

Raman spectroscopy was used to probe the as-produced material for the different precursor amounts. Typical examples are presented in figure 3. All samples presented a D peak (~1350 cm^{-1}), a G peak (~1580 cm^{-1}) and a 2D mode (~2700 cm^{-1}) [28]. As one increases the precursor content the peaks in the Raman spectra show changes. For the sample produced using 0.5 mg of precursor, the D mode is relatively low and the G mode well defined indicating a high crystallinity [25]. The 2D mode is symmetrical with full width at half maximum (FWHM) of 34 cm^{-1}. The narrow and symmetrical 2D mode and the fact that it is more intense than the G mode indicate monolayer graphene (figures 3(a) and S2(a)) [27, 29, 30]. Moreover, the G and 2D peaks that usually appear at ~1580 and 2700 cm^{-1} have undergone a blue and red shift 14 cm^{-1} and 55 cm^{-1}, respectively, which can be attributed to doping. [28, 31] This is further confirmed by presence of the D band and D' band (adjacent to the G mode) presence that arise due to defects and doping [30, 31]. However, these bands

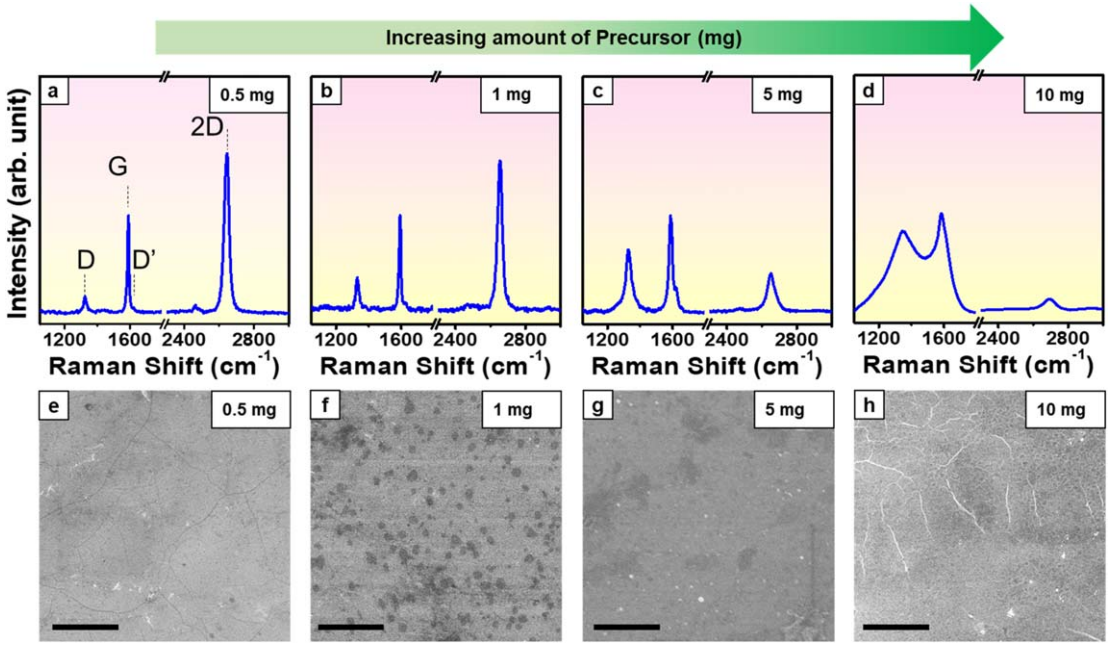

Figure 3. Characterization of the hetero-doped graphene (a to d) Raman spectra with (a) 0.5 mg (b) 1 mg (c) 5 mg (d) 10 mg precursor amounts. (e) to (h) respective SEM micrographs. Scale bar = 10 μm. Growth conditions: growth duration 3 min, initial Ar flushing 30 min and precursor decomposed at 380 °C in half closed inner quartz tube. All peaks intensities are normalized with respect to the G mode.

are not very intense suggesting perhaps the doping levels are limited. Raman area mapping of 2D/G ratio was conducted for the monolayer heterodoped graphene samples. The greater area with low 2D/G ratio in hetero-doped graphene corresponds to higher carrier concentration due to dopant atoms (figure S3(a)) [6]. The 2D width or FWHM is largely homogenous. (figure S3(b)). Moreover, the defect density can be found by G/D ratio where some spots show low G/D and some high G/D within the heterodoped graphene suggesting the non-uniform defect distribution as well as surface contamination [6, 9]. Additional Raman mapping data has been provided in figure S3. The SEM data indicates large area homogenous monolayer graphene (figure 3(e)).

Upon increasing the precursor amount to 1 mg the Raman data suggests the graphene is still primarily mono-layered. This is evidenced by 2D/G ratio (figure 3(b)) and a 2D peak FWHM value of 35 cm^{-1} (figure S4(a)). The position of G and 2D bands remained the same. However, in this case the D and D' bands (figure 3(b)) are more prominent. This effect is manifested in a lowered G/D ratio (figure S2(a)). The SEM images show small secondary graphene islands forming over the initial graphene layer (figure 3(f)). The presence of these island may contribute to the increased D and D' mode since edges are also, in effect, defects [32].

For precursor amounts of 5 mg symmetry of the 2D mode is no longer present and its intensity is less than that of the G mode (figure 3(c)). This suggests the material is few-layer graphene [31, 33]. This is also confirmed by the SEM data in which multilayers are easily observed, as for example in figure 3(g).

With a precursor amount increased to 10 mg the D, and G modes broaden significantly and the intensity of 2D peak drastically decreases relative to the G mode. These changes reflect multi-layered turbostratic multi-layer graphene formation with poor crystallinity, *viz*. highly defective graphitic material (figure 3(d)) [34, 35]. Moreover, the corresponding SEM image shows cracked pattern characteristic of multilayered graphene as shown in figure 3(h) [36]. The studies on the growth dependence with respect to the precursor mass show one can control the layer number by adjusting the precursor mass.

We also explored the role of growth time. In these studies, the precursor amount was kept at 0.5 mg. The explored growth times were 3, 5 and 7 min. The Raman data for a growth period of 3 min is presented in figure 4(a). The data, identical to that for figure 3(a), shows homogeneous mono-layer graphene growth which is also confirmed by the SEM micrographs, e.g. figure 4(d).

However, on increasing the growth time to 5 min, the D and D′ mode increase in intensity relative to the G mode indicating an increase in defects. The 2D mode decreases relative the G mode indicating few-layer graphene. These features can be seen in figure 4(b). The corresponding SEM data, e.g. figure 4(e) indicate homogeneous few-layer graphene formation. A similar trend, suggesting even more layer formation after 7 min' growth time is observed, as shown in figures 4(c) and (f). In summary, the growth time investigations show that as one increases the growth time so do the number of layers. This means growth time is also a reaction parameter to control the layer number.

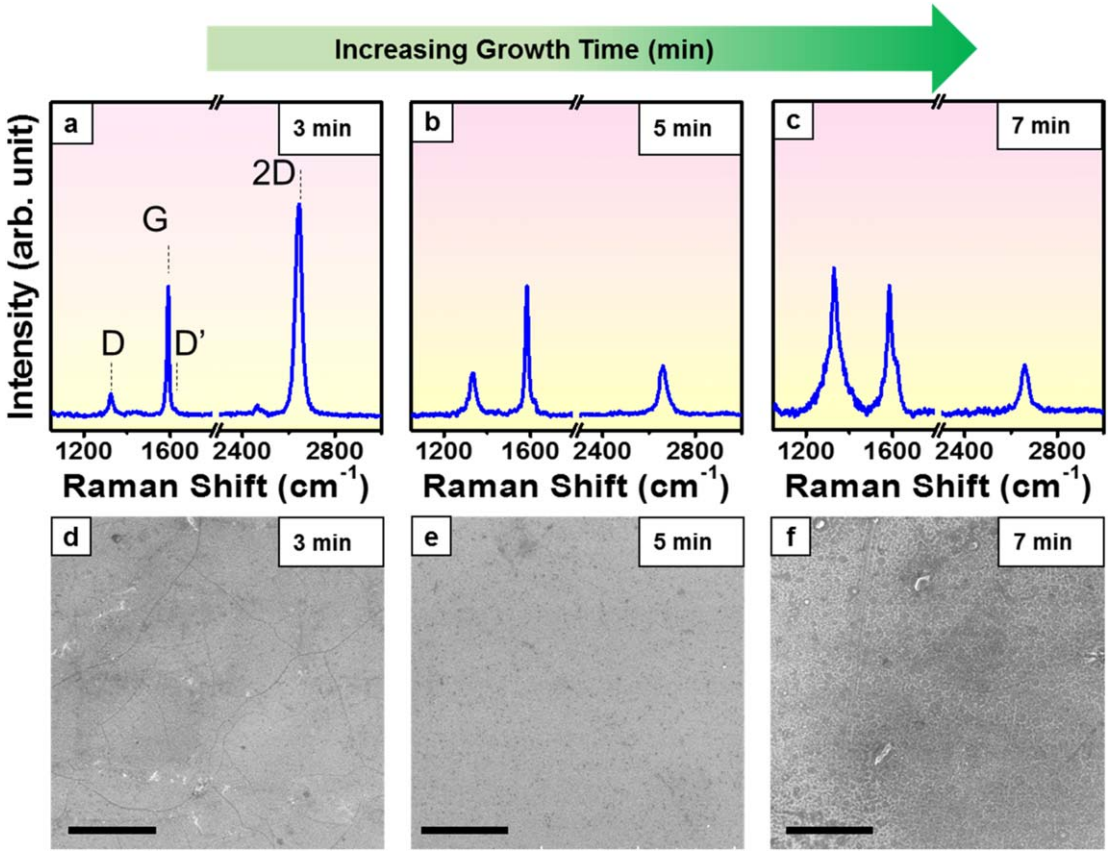

Figure 4. Characterization of the hetero-doped graphene (a to c) Raman spectra for (a) 3 min (b) 5 min (c) 7 min growth duration. (d) to (f) respective SEM micrographs. Scale bar = 10 μm. Growth conditions: initial Ar flushing 30 min and precursor amount 0.5 mg decomposed at 380 °C in half closed inner quartz tube. All peaks intensities are normalized with respect to the G mode.

We also explore different heating zone temperatures for the precursor material as this can dictate the rate with which the precursor sublimes and decomposes, and hence can affect the feedstock concentration with respect to time. The explored temperatures were 300 °C, 380 °C and 500 °C. The growth duration and precursor amount were kept constant to 3 min and 0.5 mg respectively.

With the precursor heating zone set to 300 °C, the optical microscope images from the micro Raman spectrometer suggested incomplete coverage of graphene. When measuring graphene fragments the signal was weak (large signal to noise ratio) suggesting the graphene flakes themselves are not homogeneous. None the less the G to D ratio and the 2D to G mode suggest the fragments are graphene (figure 5(a)). This suggests that within the 3 min growth time, a 300 °C precursor temperature is too low in that insufficient feedstock species are available for full graphene coverage over the Cu substrate. The SEM studies confirm incomplete graphene coverage, e.g. figure 5(d). When adjusting the precursor heating zone to 380 °C, the Raman data confirm the formation of good quality monolayer graphene (figure 5(b)). The SEM data confirm full coverage of the substrate with graphene (figure 5(e)). On further increasing the precursor heating region temperature to 500 °C, predominantly monolayer graphene is found, with small secondary flakes on the surface, as indicated by the Raman data and SEM data (figures 5(c) and (f)) which can be attributed to an increase in feedstock concentration, *viz.*, more efficient precursor decomposition. The data suggests that the optimum precursor decomposition temperature is around 380 °C. Additional data for the different trends observed from the Raman data discussed above are presented in figures S2 and S4 in the supplementary information.

In case of the monolayer of graphene formed further characterizations by TEM were conducted (figure 6). Low magnification studies show uniform large area deposition of single layer (figure 6(a)). HRTEM studies show some defects in the graphene lattice that could be attributed to doping [37]. The corresponding Fast Fourier Transform (FFT) shows a single set of three-fold reflection spots related to monolayer graphene (figure 6(b)) [38]. Moreover, looking at the edge of the material with respect to vacuum confirms the present of single layer graphene.

To better comprehend the nature of the doping of the graphene (from N and O species) we conducted core level spectroscopy using x-ray photoelectron spectroscopic (XPS) and electron energy loss spectroscopy (EELS). We begin with the XPS studies. The low resolution long range survey spectrum (figure 7(a)) reveals a

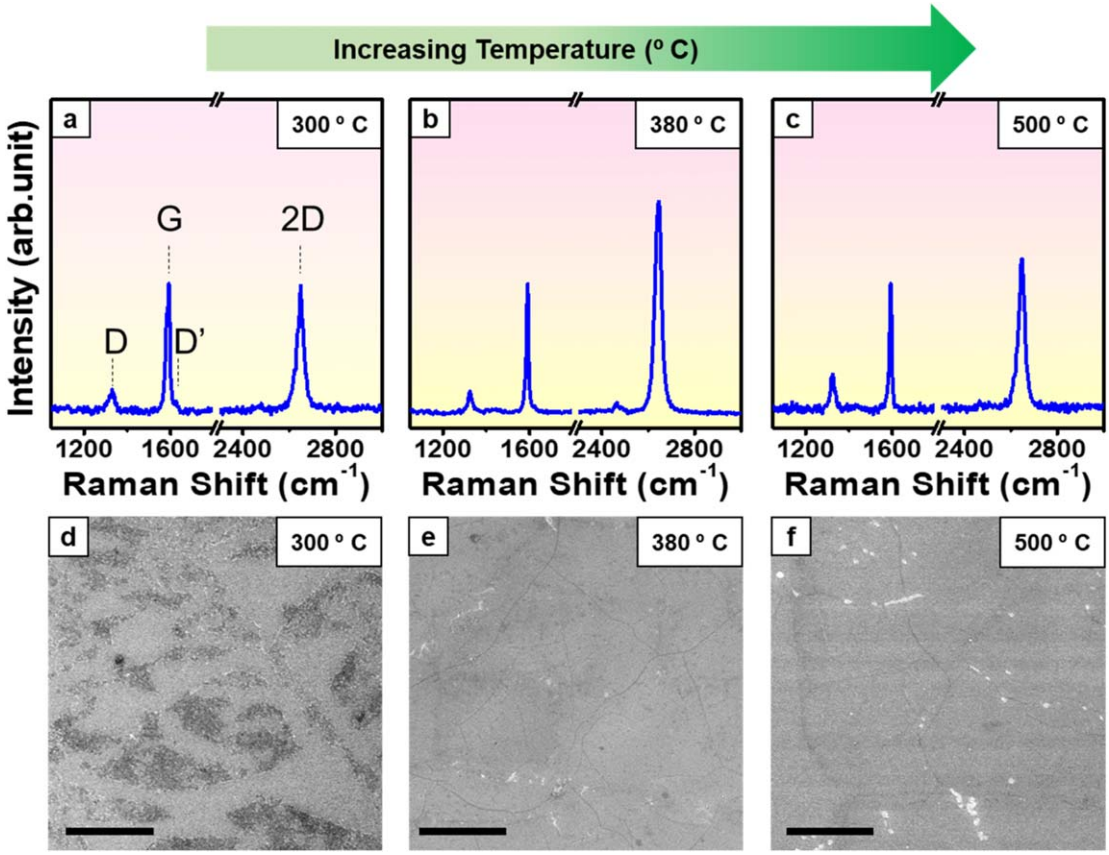

Figure 5. Characterization of the heterodoped graphene (a) to (c) Raman spectra at (a) 300 °C (b) 380 °C (c) 500 °C precursor decomposition temperatures. (d) to (f) respective SEM micrographs. Scale bar = 10 μm. Growth conditions: initial Ar flushing 30 min, growth duration 3 min, one end closed inner quartz tube and precursor amount of 0.5 mg). All peaks intensities are normalized with respect to the G mode.

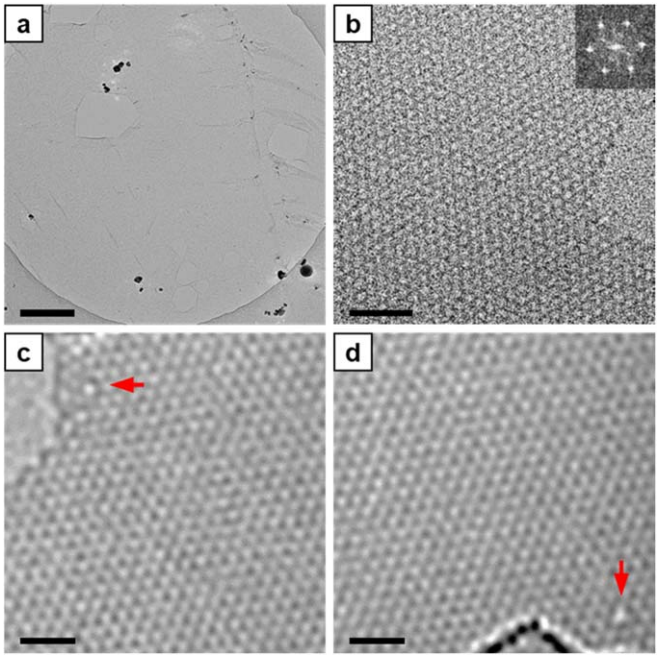

Figure 6. (a) TEM Images showing large area deposition of the hetero-doped graphene sheet on TEM copper grid. Scale bar 500 nm. (b) HRTEM images showing that the hetero-doped graphene is single layer. Scale bar = 2 nm. Inset shows respective FFT with single set of 6-fold reflection spots. (c) and (d) HRTEM Images showing defects pointed with arrows. Scale bar 1 nm.

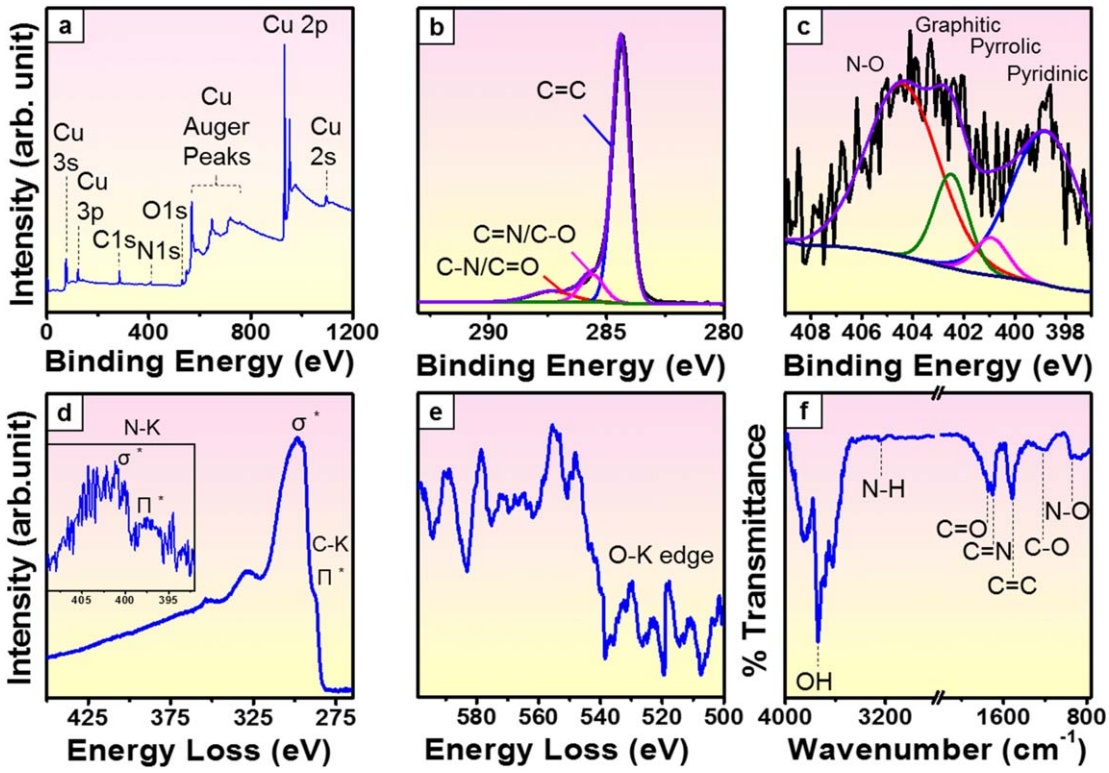

Figure 7. Characterization of the hetero-doped graphene with optimized conditions; i.e., 3 min growth duration, initial Ar flushing for 30 min, 0.5 mg precursor amount decomposed at 380 °C in one end closed inner quartz tube (a) XPS Survey spectra (b) High resolution N1s spectra (c) High resolution C1s spectra (d) EELS spectra showing Nitrogen and Carbon (e) EELS spectrum of Oxygen (f) ATR spectrum in transmission mode showing presence of different functionalities.

predominant graphitic peak at 284.3 eV and additional peaks at 402.7 eV and 531 eV corresponding to the N1s and O1s electronic transitions respectively [6, 39] and the Cu 2p peak at 932 eV [40]. The atomic percentage of N and O was determined to be 2.9% and 8.4% respectively.

The high resolution C1s main peak (figure 7(b)) can be fitted into three components centered at 284.3, 285.6 and 287.1 eV that can be ascribed to C=C, C=N/C–O and C–N/C=O respectively [6, 39]. The high resolution O1s peak (figure S5(a)) fitted into two sub peaks at 531.5 and 530.3 eV corresponding to C=O/N–O and organic C–O respectively [41, 42]. The high resolution N1s spectrum (figure 7(c)) was used to determine the different N functionalities. The spectrum shows presence of four components. The peaks are assigned to pyridinic N (398.8 eV), pyrrolic N (400.8 eV) and graphitic N (402.5 eV) [6, 43]. The fourth peak at the higher binding energy 404.3 eV is assigned to pyridinic N-oxide [43]. However, in the same range of binding energies sometimes clustered N substitutions and N_2 could also be present [44]. However, N_2 species are unlikely in this case as the samples were annealed prior to measurement. Moreover, NO_2 species are also ruled out as there is no signature for NO_2 above 405 eV [45].

The XPS spectra were obtained with the hetero-doped graphene still on the copper foil, i.e. as-produced samples. The high resolution XPS spectrum for Cu2p (figure S5(b)) shows absence of any higher oxidation metal oxide peak that usually arise in the form of a shake-up bands in the Cu2p spectrum [46]. Furthermore, the absence of a peak at the higher binding energy of ~537 eV shows no contribution from chemisorbed oxygen species [47]. This also indicates the homogeneous and large area nature of the as-produced graphene. More importantly the XPS data confirms the hetero doping of the graphene with O and N in a variety of configurations. To further confirm the doping with O and N species, we implemented EELS. Figure 6(d) shows a prominent Carbon K edge at 284.5 and 295.5 eV that arise from electronic transitions from the 1 s core level to unoccupied empty high energy π^* and σ^* states above the Fermi level respectively indicating sp^2 hybridized carbon [48].

Moreover, the N K edge shows a π^* peak at 397.7 and σ^* at 401.2 eV as seen in the inset of figure 6(d) that corresponds to sp^2 bound N in a hexagonal conformation and substitutional N, respectively [48, 49]. The O-K edge present at ~531 eV indicates oxygen atoms bound to carbon atoms [50].

We additionally look at the functional groups (doping) of the hetero-doped graphene with FTIR. In the FTIR spectrum (figure 7(f)) the peaks at ~1213 cm^{-1} and ~1110 can be attributed to C–O and N–O vibrations, respectively [51–53]. The peak at 1531 cm^{-1} is due to the C=C stretching mode and appears as a strong peak

Table 2. Summary of the different functionalities for the hetero-doped graphene developed in this work.

Functionalities
C=N, C–O, C–N, C=O, N–O, Pyrrolic, Pyridinic and Quaternary N

[51]. The presence of C=O species can also be confirmed from strong absorption at 1745 cm^{-1} [53]. The other prominent peak at 1650 cm^{-1} arises from C=N [54]. Moreover, in the region above 3200 N–H group absorbs at 3230 cm^{-1} [54]. From 3600 to 3700 cm^{-1} absorption due to OH functional groups give rise to an intense and broad peak [39]. This OH peak was also observed in the pure undoped graphene sample that was used as a control as shown in figure S5(c) which is attributed to the absorption from the ambient. Therefore, the possibility of the OH group presence being a part of heterodoped graphene structure from synthesis can be ruled out.

Thus, the XPS, EELS and FTIR data all confirm a variety of different doping configurations with N and O as indicated in table 2. They conform the direct single step synthesis of hetero-doped graphene with N and O species.

Finally, we also examined the sheet resistance of the hetero-doped graphene sheets, produced under different synthesis conditions, using the four probe method. For the different precursor masses the sheet resistance increase with increasing precursor amount as shown in figure S6(a). This correlates with the Raman spectroscopy data that shows as the precursor mass increases so does the intensity of the D and D' bands suggesting an increase in defects. Defects in graphene such as vacancies, dopants and grain boundaries all serve a scattering sites for electrons thereby decreasing conductivity and increasing the resistance [55, 56].

Similarly, with increasing growth times (figure S6(b)) the sheet resistance values correlate with the Raman D and D' modes trend. Increased growth times lead to an increase in the number of defects. For different precursor heating zone temperatures, the corresponding sheet resistance (figure S6(c)) is highest for the low temperature of 300 °C where there is incomplete coverage of the hetero-doped graphene, while for higher temperature with complete coverage the sheet resistance is reduced.

4. Conclusions

In summary, we have synthesized large area single- and few- layer highly crystalline hetero-doped graphene with both oxygen and nitrogen based species, for the first time, in a one-step thermal LPCVD approach. The synthesis step reported here is also a first in that we demonstrate hetero doping can be achieved using a *single* solid precursor as the C and multi elemental feedstock. The different synthesis parameters of growth time, precursor mass and precursor heating zone temperature and inner tube configuration were carefully studied. They show how one can use these parameters to tailor the number of layers. The data highlight the multi doping nature of the graphene which is important for catalytic applications.

Acknowledgments

This work is supported by the National Science Foundation China (NSFC, Project 51672181), the National Science Center for the financial support within the frame of the Sonata Program (Grant agreement 2014/13/D/ST5/02853) and the Opus program (Grant agreement 2015/19/B/ST5/03399). MHR thanks the Sino-German Research Institute for support (project: GZ 1400).

Notes

The authors declare no competing interests.

ORCID iDs

Zahida P Malik https://orcid.org/0000-0002-1212-6845
Mark H Rümmeli https://orcid.org/0000-0002-4448-1569

References

[1] Navalon S, Dhakshinamoorthy A, Alvaro M and Garcia H 2014 Carbocatalysis by graphene-based materials *Chem. Rev.* **114** 6179–212

[2] Novoselov K S, Geim A K, Morozov S V, Jiang D, Katsnelson M I, Grigorieva I V, Dubonos S V and Firsov A A 2005 Two-dimensional gas of massless dirac fermions in graphene *Nature* **438** 197–200
[3] Xia B Y, Yan Y, Wang X and Lou W X 2014 Recent progress on graphene-based hybrid electrocatalysts *Mater. Horiz.* **1** 379–99
[4] Su C *et al* Probing the catalytic activity of porous graphene oxide and the origin of this behaviour *Nat. Commun.* 2012 **3** 1–9
[5] Fan X, Zhang G and Zhang F 2015 Multiple roles of graphene in heterogeneous catalysis *Chem. Soc. Rev.* **44** 3023–35
[6] Wang H, Maiyalagan T and Wang X 2012 Review on recent progress in nitrogen-doped graphene: synthesis, characterization, and its potential applications *ACS Catal.* **2** 781–94
[7] Dreyer D R, Jia H-P and Bielawski C W 2010 Graphene oxide: a convenient carbocatalyst for facilitating oxidation and hydration reactions *Angew. Chem.* **122** 6965–8
[8] Duan X, Donnell K O, Sun H, Wang Y and Wang S 2015 Sulfur and nitrogen co-doped graphene for metal-free catalytic oxidation reactions *Small* **11** 3036–44
[9] Chang C-K *et al* Band gap engineering of chemical vapor deposited graphene by *in situ* BN doping *ACS Nano* 2013 **7** 1333–41
[10] Bepete G, Voiry D, Chhowalla M, Chiguvare Z and Coville N J 2013 Incorporation of Small BN Domains in Graphene During CVD Using Methane, Boric acid and Nitrogen gas *Nanoscale* **5** 6552–7
[11] Ma X, Ning G, Qi C, Xu C and Gao J 2014 Phosphorus and nitrogen dual-doped few-layered porous graphene: a high-performance anode material for lithium-ion batteries *ACS Appl. Mater. Interfaces* **6** 14415–22
[12] Xu J, Dong G, Jin C, Huang M and Guan L 2013 Sulfur and nitrogen co-doped, few-layered graphene oxide as a highly efficient electrocatalyst for the oxygen- reduction reaction *Chem. Sus. Chem.* **6** 493–9
[13] Xue Y, Yu D, Dai L, Wang R, Li D, Roy A, Lu F, Chen H, Liu Y and Qu J 2013 Three-dimensional b, n-doped graphene foam as a metal-free catalyst for oxygen reduction reaction *Phys.Chem. Chem. Phys.* **15** 12220–6
[14] Choi C H, Chung M W, Park S H and Woo S I 2013 Additional doping of phosphorus and/or sulfur into nitrogen-doped carbon for efficient oxygen reduction reaction in acidic media *Phys. Chem. Chem. Phys.* **15** 1802–5
[15] Liang J, Jiao Y, Jaroniec M and Qiao S Z 2012 Sulfur and nitrogen dual-doped mesoporous graphene electrocatalyst for oxygen reduction with synergistically enhanced performance *Angew. Chem. Int. Ed.* **51** 11496–500
[16] Wang Z-L, Xu D, Xu J-J and Zhang X-B 2014 Oxygen electrocatalysts in metal–air batteries: from aqueous to nonaqueous electrolytes *Chem. Soc. Rev.* **43** 7746–86
[17] Silva R, Voiry D, Chhowalla M and Asefa T 2013 Efficient metal-free electrocatalysts for oxygen reduction: polyaniline-derived n- and o-doped mesoporous carbons *J. Am. Chem. Soc.* **135** 7823–6
[18] Chen S, Duan J, Jaroniec M and Qiao S-Z 2014 Nitrogen and oxygen dual-doped carbon hydrogel film as a substrate-free electrode for highly efficient oxygen evolution reaction *Adv. Mater.* **26** 2925–30
[19] Wang X, Sun G, Routh P, Kim D-H, Huang W and Chen P 2014 Heteroatom-doped graphene materials: syntheses, properties and applications *Chem. Soc. Rev.* **43** 7067–98
[20] Paraknowitsch J P and Thomas A 2013 Doping carbons beyond nitrogen: an overview of advanced heteroatom doped carbons with boron, sulphur and phosphorus for energy applications *Energy Environ. Sci.* **6** 2839–55
[21] Barreiro A *et al* Thermal decomposition of ferrocene as a method for production of single-walled carbon nanotubes without additional carbon sources *J. Phys. Chem. B.* 2006 **110** 20973–7
[22] Pilatos G *et al* Graphene by one-step chemical vapor deposition from ferrocene vapors: properties and electrochemical evaluation *J. App. Phys.* 2016 **119** 064303
[23] Nawaz H, Akhter Z, Yameen S, Siddiqi H M, Mirza B and Rifat A 2009 Synthesis and biological evaluations of some schiff-base esters of ferrocenyl aniline and simple aniline *J. Organomet. Chem.* **694** 2198–203
[24] Seo J, Lee J, Jang A-R, Choi Y, Kim U, Shin H S and Park H 2017 Study of cooling rate on the growth of graphene via chemical vapor deposition *Chem. Mater.* **29** 4202–8
[25] Ta H Q, Perello D J, Duong D L, Han G H, Gorantla S, Nguyen V L, Bachmatiuk A, Rotkin S V, Lee Y H and Rümmeli M H 2016 Stranski−krastanov and volmer−weber CVD growth regimes to control the stacking order in bilayer graphene *Nano Lett.* **16** 6403–10
[26] Rümmeli M H, Gorantla S, Bachmatiuk A, Phieler J, Geißler N, Ibrahim I, Pang J and Eckert J 2013 On the role of vapor trapping for chemical vapor deposition (CVD) grown graphene over copper *Chem. Mater.* **25** 4861–6
[27] Hao Y, Wang Y, Wang L, Ni Z, Wang Z, Wang R, Koo C K, Shen Z and Thong J T L 2010 Probing layer number and stacking order of few-layer graphene by raman spectroscopy *Small* **6** 195–200
[28] Childres I, Jaureguib L A, Park W, Caoa H and Chena Y P 2013 *Raman Spectroscopy of Graphene and Related Materials.* (New York: Nova Science Publishers) p 1–20
[29] Das A *et al* Monitoring dopants by raman scattering in an electrochemically top-gated graphene transistor *Nat. Nanotechnol.* 2008 **3** 210–5
[30] Sun Z, Yan Z, Yao J, Beitler E, Yu Z and Tour J M 2010 Growth of graphene from solid carbon sources *Nature* **468** 549–52
[31] Podila R, Chacón-Torres J, Spear J T, Pichler T and Ayala P 2012 Spectroscopic investigation of nitrogen doped graphene *App. Phys. Lett.* **101** 123108(1)- 123108(4)
[32] Rummeli M H, Bachmatiuk A, Scott A, Borrnert F, Warner J H, Hoffman V, Lin J-H, Cuniberti G and Buchner B 2010 Direct low-temperature nanographene CVD synthesis over a dielectric insulator *ACS Nano* **4** 4206–10
[33] Gupta A, Chen G, Joshi P, Tadigadapa S and Eklund P C 2006 Raman scattering from high-frequency phonons in supported n-graphene layer films *Nano Lett.* **6** 2667–73
[34] Ferrari A C *et al* Raman spectrum of graphene and graphene layers *Phys. Rev. Lett.* 2006 **97** 187401(1)- 187401(4)
[35] Lu Y-F, Lo S-T, Lin J-C, Zhang W, Lu J-Y, Liu F-H, Tseng C-M, Lee Y-H, Liang C-T and Li L-J 2013 Nitrogen-doped graphene sheets grown by chemical vapor deposition: synthesis and influence of nitrogen impurities on carrier transport *ACS Nano* **7** 6522–32
[36] Jang B, Kim B, Kim J-H, Lee H-J, Sumigawa T and Kitamura T 2017 Asynchronous cracking with dissimilar paths in multilayer graphene *Nanoscale* **9** 17325–33
[37] Shinde S M, Kano E, Kalita G, Takeguchi M, Hashimoto A and Tanemura M 2016 Grain Structures of Nitrogen-Doped Graphene Synthesized by Solid Source-Based Chemical Vapor Deposition *Carbon* **96** 448–53
[38] Limbu T B, Hernández J C, Mendoza F, Katiyar R K, Razink J J, Makarov V I, Weiner B R and Morell G 2018 A novel approach to the layer-number-controlled and grain-size-controlled growth of high quality graphene for nanoelectronics *ACS Appl. Nano Mater.* **1** 1502–12
[39] Lin Z, Waller G, Liu Y, Liu M and Wong C-P 2012 Facile synthesis of nitrogen-doped graphene via pyrolysis of graphene oxide and urea, and its electrocatalytic activity toward the oxygen-reduction reaction *Adv. Energy Mater.* **2** 884–8
[40] Mallineni S S K *et al* Influence of dopants on the impermeability of graphene *Nanoscale* 2017 **9** 6145–50

[41] Sun X, Brückner C and Lei Y 2015 One-pot and ultrafast synthesis of nitrogen and phosphorus Co-Doped carbon dots possessing bright dual wavelength fluorescence emission *Nanoscale* **7** 17278–82
[42] Zhang J, Li C, Peng Z, Liu Y, Zhang J, Liu Z and Li D 2017 3D free-standing nitrogen-doped reduced graphene oxide aerogel as anode material for sodium ion batteries with enhanced sodium storage *Sci. Rep.* **7** 4886
[43] Biddinger E J, Deak D V and Ozkan U S 2009 Nitrogen-containing carbon nanostructures as oxygen-reduction catalysts *Top Catal.* **52** 1566–74
[44] Susi T, Pichler T and Ayala P 2015 X-ray photoelectron spectroscopy of graphitic carbon nanomaterials doped with heteroatoms *J. Nanotechnol.* **6** 177–92
[45] Lund T, Nguyen P T and Ruhland T 2015 Electrochemical grafting of TiO_2-based photo-anodes and its effect in dye-sensitized solar cells *J. Electroanal. Chem.* **758** 85–92
[46] Hayez V, Franquet A, Hubin A and Terryn H 2004 XPS Study of the atmospheric corrosion of copper alloys of archaeological interest *Surf. Interface Anal.* **36** 876–9
[47] Nasini U B, Bairi V G, Ramasahayama S K, Bourdo S E, Viswanathan T and Shaikh A U 2014 Phosphorous and nitrogen dual heteroatom doped mesoporous carbon synthesized via microwave method for supercapacitor application *J. Power Sources* **250** 257–65
[48] Arenal R, March K, Ewels C P, Rocquefelte X, Kociak M, Loiseau A and Stéphan O 2014 Atomic configuration of nitrogen-doped single-walled carbon nanotubes *Nano Lett.* **14** 5509–16
[49] Lin Y, Pan X, Qi W, Zhang B and Su D S 2014 Nitrogen-doped onion-like carbon: a novel and efficient metal-free catalyst for epoxidation reaction *J. Mater. Chem. A* **2** 12475–83
[50] Angelo D D, Bongiorno C, Amato M, Deretzis I, Magna A L, Fazio E and Scalese S 2017 Oxygen functionalities evolution in thermally treated graphene oxide featured by EELS and DFT calculations *J. Phys. Chem. C* **121** 5408–14
[51] Kantcheva M and Ciftlikli E Z 2002 FTIR spectroscopic characterization of NOx species adsorbed on ZrO_2 and ZrO_2-SO_4^{2-} *J. Phys. Chem. B* **106** 3941–9
[52] Ma G, Huang K, Ma J-S, Ju Z, Xing Z and Zhuang Q-C 2017 Phosphorus and oxygen dual-doped graphene as superior anode material for room-temperature potassium-ion batteries . *J. Mater. Chem. A* **5** 7854
[53] Pavia D L, Lampman G M, Kriz G S and Vyvyan J R 2013 *Introduction to Spectroscopy* (Cengage Learning) p 20
[54] Li O L, Chibab S, Wada Y, Panomsuwancd G and Ishizaki T 2017 Synthesis of graphitic-N and amino-N in nitrogen-doped carbon via solution plasma process and exploration of their synergic effect for advanced oxygen reduction reaction *J. Mater. Chem. A* **5** 2073–82
[55] Banhart F, Kotakoski J and Krasheninnikov A V 2011 Structural defects in graphene *ACS Nano* **5** 26–41
[56] Wehling T O, Yuan S, Lichtenstein A I, Geim A K and Katsnelson M I 2010 Resonant scattering by realistic impurities in graphene *Phys. Rev. Lett.* **105** 056802